FACTA UNIVERSITATIS
Series: **Electronics and Energetics** Vol. 39, N° 1, March 2026, pp. 285 - 306
https://doi.org/10.2298/FUEE2601285F

Original scientific paper

IN-SITU DIGITAL TWINNING OF INDUCTION MACHINES VIA SENSITIVITY-BASED GENETIC ALGORITHM PARAMETER ESTIMATION

Filip Filipović, Anđela Stojiljković, Nebojša Mitrović, Bojan Banković, Milutin Petronijević, Vojkan Kostić

[1]University of Niš, Faculty of Electronic Engineering, Department of Power Engineering, Republic of Serbia

ORCID iDs:	Filip Filipović	https://orcid.org/0000-0002-1930-9273
	Anđela Stojiljković	https://orcid.org/0009-0009-2532-1859
	Nebojša Mitrović	https://orcid.org/0000-0003-3767-3244
	Bojan Banković	https://orcid.org/0000-0002-5504-599X
	Milutin Petronijević	https://orcid.org/0000-0003-2396-0891
	Vojkan Kostić	https://orcid.org/0000-0002-7714-469X

Abstract. *This paper presents a novel, non-invasive methodology for creating a high-fidelity digital twin using only steady-state operational data. The proposed approach employs a four-step workflow with two-stage parameter identification algorithm. First, a grid-based sensitivity analysis is conducted to establish robust and constrained search boundaries. Subsequently, a genetic algorithm performs a precise search within these boundaries to identify the final T-equivalent circuit parameters. The methodology was validated on a 1.5 kW induction motor. All but core loss identified parameters demonstrated similarity with those obtained from standard offline tests, and the resulting digital twin accurately reproduced the machine's behaviour when compared to experimental measurements.*

Key words: *induction machine, sensitivity analysis, genetic algorithm, digital twin, in-situ*

1. INTRODUCTION

Reliable operation of industrial processes is paramount in modern industry. Induction Machines (IMs) remain indispensable workhorses and key components in industry, powering everything from pumps and fans to complex machines. Consequently, ensuring their operational health, performance and efficiency through modern methods like condition monitoring and predictive maintenance becomes a necessity, rather than a luxury [1], [2]. The key technology in this domain is the Digital Twin (DT), which provides a high-fidelity, virtual

Received July 17, 2025; revised September 10, 2025; accepted September 21, 2025
Corresponding author: Filip Filipović
University of Niš, Faculty of Electronic Engineering, Department of Power Engineering, Aleksandra Medvedeva 4, 18104 Niš, Republic of Serbia
E-mail: filip.filipovic@elfak.ni.ac.rs

representation of a physical asset [3]. An accurate DT of IM allows for real-time performance analysis, fault diagnostics and control strategy optimisation without interfering with the physical machine [4].

The fidelity of IM's DT is fundamentally dependent on the accuracy of its model parameters. The widely accepted modelling of IM that accurately represents steady-state and dynamic behaviour, shown in Fig. 1, uses a T-equivalent circuit. However, obtaining the parameters of T-equivalent circuit – stator and rotor resistance (R_s, R_r), stator and rotor leakage inductance (λ_s, λ_r), magnetising resistance and reactance (R_m, L_m), respectively – presents a significant practical challenge [5]. Based on the provided scheme, equivalent phase resistance (R_{eq}) and inductance (L_{eq}), along with active (P_{eq}) and reactive (Q_{eq}) power can be calculated as in (1-4):

$$R_{eq} = \mathrm{Re}\left\{(R_s + j\omega_{sync}\lambda_s) \oplus ((R_m \parallel j\omega_{sync}L_m) \parallel (\frac{R_r}{s} + j\omega_{sync}\lambda_r))\right\} \tag{1}$$

$$L_{eq} = \mathrm{Im}\left\{(R_s + j\omega_{sync}\lambda_s) \oplus ((R_m \parallel j\omega_{sync}L_m) \parallel (\frac{R_r}{s} + j\omega_{sync}\lambda_r))\right\}\frac{1}{\omega_{sync}} \tag{2}$$

$$P_{eq} = 3R_{eq}I_{eq,eff}^2 \tag{3}$$

$$Q_{eq} = 3L_{eq}\omega_{sync}I_{eq,eff}^2 \tag{4}$$

where S is slip and ω_{sync} is synchronous speed, $\oplus$ denotes series connection of impedance, and $\parallel$ denotes parallel connection of impedance.

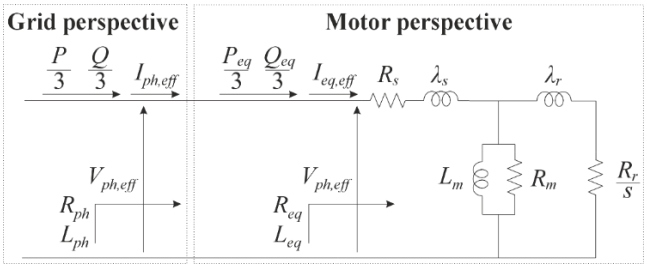

Fig. 1 T-equivalent circuit of induction machine

The conventional and most standardised method for parameter determination involves conducting a series of offline tests, namely no-load and locked-rotor tests, as prescribed by the IEEE 112 [6]. While these tests are accurate, their proper conduct imposes a practical challenge. They necessitate decoupling the machine from its load and coupling it to another machine that will rotate the rotor with synchronous speed in one test, and blocking the rotor from turning in another test. Also, there is a necessity for voltage reduction equipment during the locked-rotor test, or the usage of equipment that can withstand current several times nominal. This is impractical for critical machinery or imposes a daunting task concerning the significance of the machine for some auxiliary tasks. Mentioned problems create a strong demand for non-invasive parameter identification techniques.

When a medium- or high-performance Variable Frequency Drive (VFD) is used for control of IM, it will conduct parameter identification [7] to enable reliable and efficient operation [8]. Furthermore, when new IMs are purchased, many manufacturers will provide datasheets with sufficient data to do a rough estimation of required parameters [9]. However, these scenarios do not cover a vast number of motors currently in service. A significant challenge arises for legacy machines that have been operating for years or have undergone repairs and rewinding, which invalidates their original nameplate data. Additionally, many of these motors are part of installations that lack modern VFDs capable of performing auto-tuning. This results in a population of machines with unknown parameters, hindering the implementation of advanced control or condition monitoring strategies.

Everything previously mentioned can distinguish one group of IMs that is not favourable for the creation of DT, directly connected with limited nameplate data (due to rewinding or age), that powers some auxiliary non-critical function. This paper proposes a two-stage approach for determining IM parameters using only recorded voltages, current and speed in the stationary state. The only required parameter is rated speed (for slip calculation). Parameters are determined in-situ, without the need for IM decoupling.

The parameter estimation using in-situ methods is well-researched and documented. Field studies document how practical constraints motivate in-situ techniques beyond laboratory IEEE Std 112 tests, and analyze error sources when motors remain coupled to their loads [10]. Some online approaches rely on techniques like the Extended Kalman Filter (EKF) or Recursive Least Squares to track parameter variations [11]. Recently, the use of artificial intelligence and metaheuristic optimisation algorithms has garnered considerable attention for its ability to solve complex, multi-modal problems [12]. Algorithms such as Particle Swarm Optimisation (PSO) and Genetic Algorithms (GA) have been successfully applied to IM parameter identification [13], [14], [15]. Also, parameter estimation using a hybrid approach is popular in literature [16]. All those algorithms find application in analysis of stationary points [17], and transient states [18]. However, a significant portion of this research, especially that employing metaheuristic algorithms, still relies on data derived from the standard offline no-load and locked-rotor tests to formulate the objective function [13], [19]. The usual application of in-situ methods is to assess IM efficiency [14], [15], [20], [21], [22], and DTs include detail physical, mechanical, thermal and electrical model [23], [24], [25]. This work targets a practical gap for directly grid-connected induction motors: in many critical installations, there is no non-invasive, always-on way to validate machine parameters and detect faults during normal operation. By pairing modest instrumentation (voltage/current acquisition and an encoder) with an in-situ, steady-state digital twin, the supervised drive or plant controller can track residuals between measured and modeled quantities and flag irregular operating states—for example, unexpected load increase due to jamming/bearing degradation or load loss from belt slip/snap. The approach enables continuous condition awareness and faster diagnostics without process interruption, which is particularly valuable for closed, hard-to-access systems where periodic offline tests are impractical. In short, the method converts routine measurements into actionable health signals for grid-fed IMs, bridging the gap between traditional nameplate-based monitoring and full VFD-based analytics. Therefore, a clear need remains for a straightforward methodology that can accurately identify all machine parameters using only easily accessible, steady-state operational data without any process interruption and its comparison with standardized tests.

To strengthen our motivation, we now quantify the practical burden of IEEE 112 tests: the no-load test requires thermal stabilization with readings at half-hour intervals, often taking several hours off-line, while locked-rotor testing must be limited to ~12 s shots and

repeats at different voltages, with ~6–8 times rated current and corresponding safety risk [6]. In contrast, our in-situ approach uses normal operating data (no forced stalls, no decoupling), is non-intrusive, and reduces test burden to minutes of data collection with essentially no production downtime.

After signal processing and feature extraction, we use Grid Search (GS) to: confirm the existence of a meaningful minimum (sanity-check the data/model); assess how good the best achievable fit is (if the floor remains high, data quality or model form may be inadequate); support model selection/validation when alternative IM models are needed (like different leakage/core-loss treatments); and deliver tight, physically meaningful bounds and initializer seeds for the final search. Within this subspace, a GA then performs precise identification, summarized over multiple runs. This design reduces spurious local minima and improves reproducibility, without claiming formal global optimality. The identified parameters are then used to create DT in MATLAB, whose accuracy is rigorously validated against experimental data.

In this paper, the following contributions are presented:

1. A four-step workflow with two-stage in-situ identification for induction-motor T-model parameters using only readily available operational data – three-phase voltages, currents and rotational speed;
2. A bounded, sensitivity-guided search that reduces GA variance and avoids local minima;
3. Head-to-head validation against IEEE-112 parameters and baselines.

Taken together, these contributions yield a deployment-ready workflow. Before outlining the paper's structure, the study highlights practical advantages and usage guidance Engineering benefits of the proposed method include no work outage while relevant data is recorded, usage of broadly available sensors in industry, and it does not require an elaborate setup for data collection. Use IEEE 112 when a standardized acceptance report or cross-lab comparability is required. Use the proposed in-situ method for ongoing DT maintenance, after repairs, or where test downtimes and high-current stress are unacceptable. A hybrid approach is also possible: initialize from IEEE 112, then fine-tune in-situ. These usage notes clarify when each pathway is preferable in practice.

The remainder of this paper is organised as follows. The following section details the experimental setup, the data processing techniques and the proposed four-step workflow with two-stage identification algorithm. In the third section, validation results are presented, comparing the performance of the created digital twin with the physical machine. Finally, concluding remarks are stated and some suggested directions for future work are pointed out.

2. METHODOLOGY

The complete workflow for creating DT, from physical measurement to the final identified parameters, is broken down into three distinct and sequential stages to ensure clarity and repeatability. The proposed methodology for the in-situ parameter identification of the IM consists of three main stages: (2.1) the experimental data acquisition from the laboratory test bench, (2.2) the processing of raw data to calculate the key operational variables, and (2.3) the implementation of a two-stage optimization algorithm to identify the T-equivalent circuit parameters.

2.1. Experimental Setup

The experimental test bench, depicted in Fig. 2 and realised at the Laboratory for Electrical Drives at the Faculty of Electronic Engineering, University of Niš, was designed to capture high-fidelity data from an IM under various operating conditions. The test machine is a 1.5 kW Siemens 1LA7090-2AA10 induction motor, whose nameplate data is detailed in Table 1. The motor is connected directly to the three-phase 400 V, 50 Hz power grid in the laboratory.

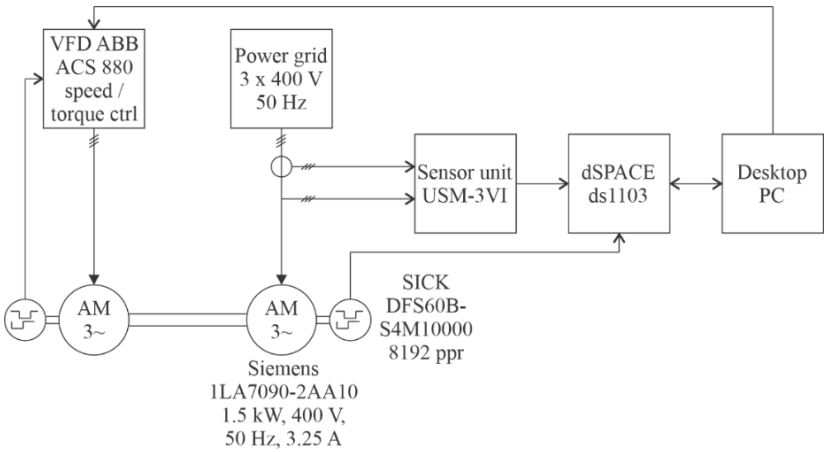

a)

b)

Fig. 2 The experimental test bench: a) functional diagram; b) laboratory setup

Phase voltages and currents are measured using a USM-3VI sensor unit placed between the grid and motor terminals. The increment of IM's rotor's position is captured using a SICK DFS60B-S4M10000 incremental encoder, programmed to output 8192 pulses per revolution. A second IM, acting as a controllable load or drive machine, is mechanically coupled to the test IM's shaft. The second IM is driven by ABB ACS880 VFD in speed- or torque-control mode and equipped with a braking resistor, thus allowing the test IM to be operated in both motor and generator regimes.

All measurement signals – three-phase voltages, three-phase currents and encoder output – are fed into a dSPACE ds1103 controller board for real-time data acquisition.

Table 1 Test IM nameplate data

Parameter	Value
Manufacturer	Siemens
Model	1LA7090-2AA10
Rated power	1.5 kW
Rated voltage	400 V
Rated current	3.25 A
Rated speed	2860 rpm
Rated frequency	50 Hz
Power factor	0.85

2.2. Data Acquisition and Processing

Three-phase voltages and currents are sampled at 10 kHz, while the mechanical rotational speed of the rotor is calculated using position increment at 1 kHz. A flowchart of signal processing is presented in Fig. 3. The machine was operated at several distinct and stable operating points, characterised by different speeds and torques. The time diagram of IM speed and synchronous speed, along with selected stable operating points, is shown in Fig. 4. For each of these points, the average value of voltage, current, power and slip were calculated to serve as input for the optimisation algorithm. The IM is loaded with toque from 0 to 5 Nm in steps of 1 Nm in both directions in first set of tests. At the start of the second test, the rotor speed is fixed at 3000 rpm, then reduced to 2960 rpm, and after that increased to 3040 rpm in steps of 20 rpm.

The core of the signal processing relies on Enhanced Phase-Locked Loop with Moving Average Filter (EPMAF-PLL Type 2), as described in [26] and [27], to accurately estimate the grid voltage angle θ and frequency ω_{sync}. Angle θ is used for Park transformation of measured voltages and currents from the *abc* to *dq* reference frame. *dq* reference frame is used because of simplified power calculation and due to instantaneous and accurate calculation of RMS values.

All measured quantities are averaged over a whole stable operating point (as depicted in Fig. 4) to mitigate the quantization error. Quantization error in this specific case has the biggest impact on the used encoder, since AD converters used for voltage and current measurement on dSpace ds1103 are 16 bit. With 8192 pulses per revolution, single-edge counting and speed calculation every 1 ms, the quantization error of slip is $\Delta s = (2\pi/(8192 \cdot 0.001))/(2\pi 50) \approx 0.24\%$ at speed close to synchronous. Those finite steps could be problematic near synchronous speed, but with averaging multiple values standard deviation of quantization noise falls by $\sqrt{N}$, where N is the number of samples for

averaging [28], [29]. Each stable operating point has several thousand recorded values for speed.

From the grid perspective, the active (P) and reactive (Q) power and RMS values of voltages and currents are then calculated from dq components using the expressions (5) and (6) in the following way:

$$P = \frac{3}{2}(V_d I_d + V_q I_q + 2V_0 I_0) \quad \wedge \quad Q = \frac{3}{2}(V_q I_d - V_d I_q) \tag{5}$$

$$V_{ph,eff} = \frac{\sqrt{V_d^2 + V_q^2}}{\sqrt{2}} \quad \wedge \quad I_{ph,eff} = \frac{\sqrt{I_d^2 + I_q^2}}{\sqrt{2}} \tag{6}$$

Using the above quantities, equivalent phase resistance (R_{ph}) and inductance (L_{ph}) as seen from the grid can be calculated as (7) and (8):

$$R_{ph} = \frac{P/3}{I_{ph,eff}^2} \tag{7}$$

$$L_{ph} = \frac{Q/3}{I_{ph,eff}^2 \omega_{sync}} \tag{8}$$

Finally, the slip S can be calculated using (9) in the following way:

$$s = \frac{\omega_{sync} - p\omega_{mec}}{\omega_{sync}} \tag{9}$$

where ω_{mec} is the mechanical rotational speed measured by the encoder, p - number of pole pairs (in this specific case $p = 1$).

These calculated values serve as the ground-truth data for the objective function in the identification algorithm. Selected quantities, for each stable operating point, are shown in Fig. 5 (stable plateaus numbering for Fig. 4 and points numbering for Fig. 5 is synchronised).

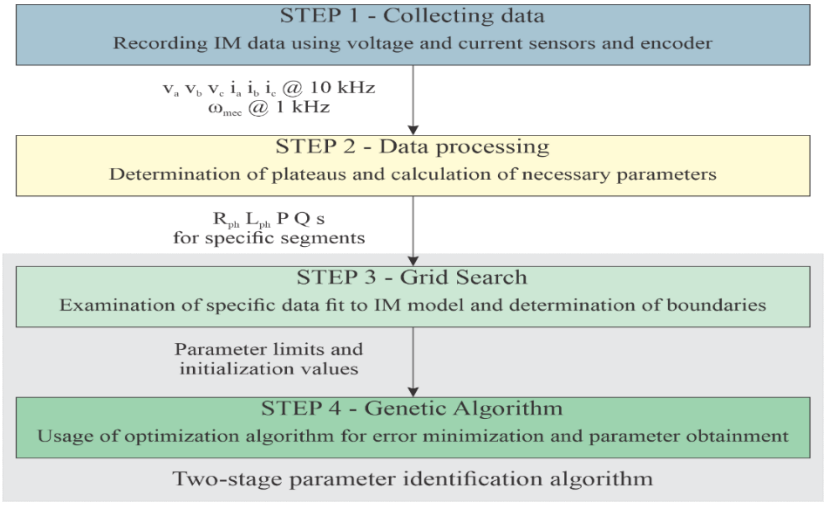

Fig. 3 Flowchart of signal processing

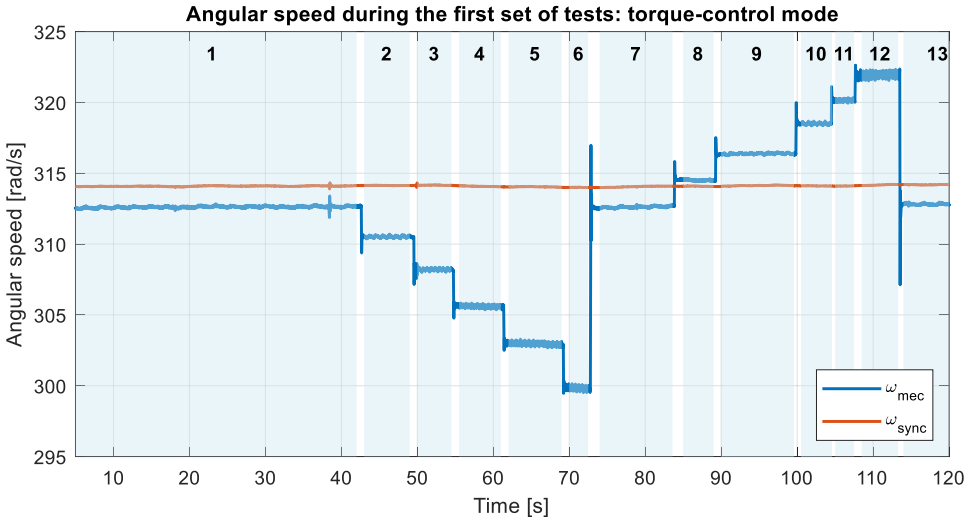

a)

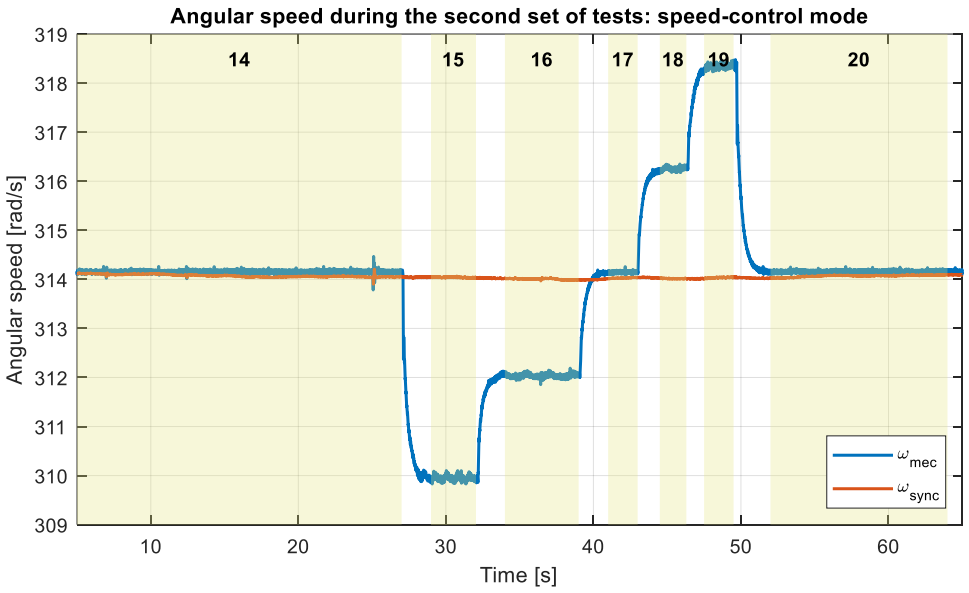

b)

Fig. 4 Time diagram of the IM speed and synchronous speed, with highlighted selected characteristic periods. The second IM is operated in a: a) torque-control mode; b) speed-control mode

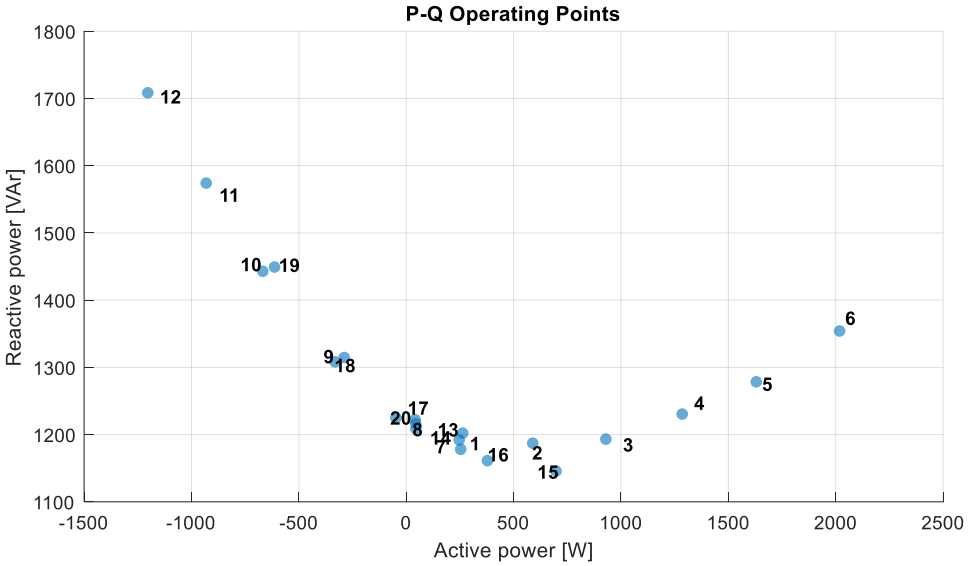

a)

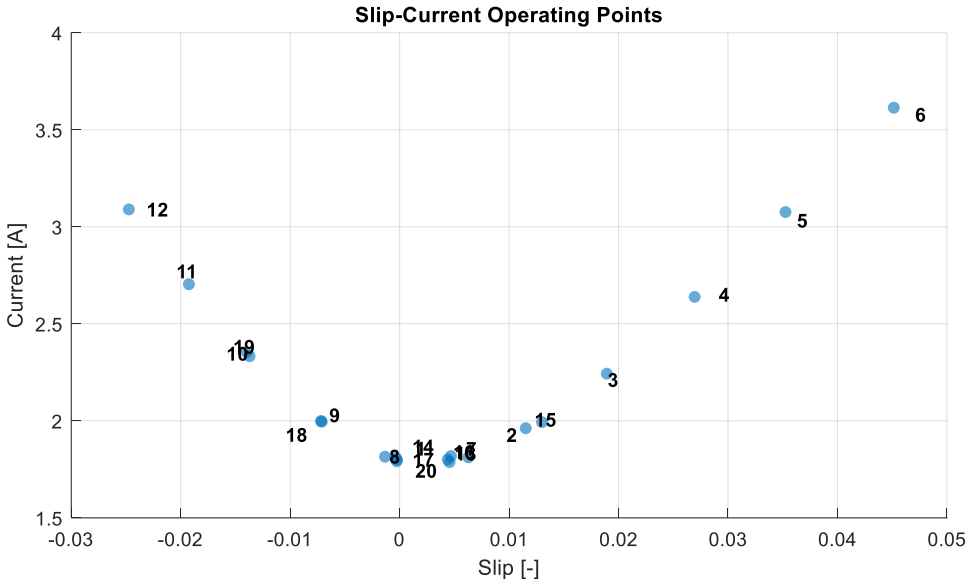

b)

Fig. 5 Selected quantities for display, for each stable operating point: a) $Q = f(P)$; b) $I_{ph,eff} = f(s)$

2.3. The Two-Stage Parameter Identification Algorithm

The algorithm's objective is to identify the six parameters of the standard T-equivalent circuit (R_s, R_r, λ_s, λ_r, R_m, L_m presented in Fig. 1). A two-stage approach was developed to ensure a robust and accurate search.

The objective function is formed to calculate the deviation between measured and calculated parameters using the standardised Root Mean Squared Error (RMSE). For any assumed set of T-circuit parameters, the model's equivalent resistance (R_{eq}), inductance (L_{eq}), current ($I_{eq,eff}$), active (P_{eq}) and reactive (Q_{eq}) power can be calculated and compared to measured values over RMSE metrics defined in (10-14):

$$\Delta_r = \sqrt{\frac{1}{N}\sum_{i=1}^{N}(R_{eq,i} - R_{ph,i})^2} \tag{10}$$

$$\Delta_l = \sqrt{\frac{1}{N}\sum_{i=1}^{N}(L_{eq,i} - L_{ph,i})^2} \tag{11}$$

$$\Delta_i = \sqrt{\frac{1}{N}\sum_{i=1}^{N}(I_{eq,eff,i} - I_{ph,eff,i})^2} \tag{12}$$

$$\Delta_p = \sqrt{\frac{1}{N}\sum_{i=1}^{N}(P_{eq,i} - P_i)^2} \tag{13}$$

$$\Delta_q = \sqrt{\frac{1}{N}\sum_{i=1}^{N}(Q_{eq,i} - Q_i)^2} \tag{14}$$

While the total error is calculated in (15) as the weighted sum of errors:

$$\Delta_{total} = w_r\Delta_r + w_l\Delta_l + w_i\Delta_i + w_p\Delta_p + w_q\Delta_q \tag{15}$$

where w_r, w_l, w_i, w_p, w_q are weighted factors.

To avoid convergence to local minima and to establish a reliable search space for the subsequent optimisation, a coarse GS was performed first. Directly applying a global optimizer like a GA to a wide, unconstrained search space for this type of multi-parameter problem can be computationally expensive and risks premature convergence. To mitigate this, based on typical values for a machine of this size [30], wide initial boundaries were set for each of the five T-circuit parameters ($\lambda_s + \lambda_r$ are considered as a single parameter). The algorithm then exhaustively calculated the five-error metrics (10)-(14) for all possible parameter combinations. A sensitivity analysis based on conditional minimisation was performed to correlate the individual objective functions with specific parameters of the T-equivalent circuit. For each parameter being examined (for example R_s), its value was systematically varied across a predefined range. At each step, an exhaustive search was conducted on the remaining four parameters to find the combination that yielded the global minimum for a single objective function (for example Δ_r). This process effectively maps out the "floor" of the error surface for each parameter, revealing not just sensitivity but the best achievable performance conditioned on that parameter's value.

By plotting the minimum error values against each parameter, clear sensitivities were observed. Those specific plots are shown in Fig. 6. As seen in Fig. 6, the resulting plots often reveal well-defined convex "valleys" for certain parameter-error pairings, which strongly indicates a clear, unimodal region containing the global minimum. This step is providing the GA with narrow, high-probability search spaces and significantly enhances its convergence speed and reduces the risk of it settling on a local minimum. The sensitivity analysis yielded the following conclusions for setting the GA boundaries:

- A strong, monotonic correlation was found between R_s and Δ_r, Δ_p and Δ_q, allowing its range to be confidently refined as $3 < R_S\ [\Omega] < 9$;
- R_r correlates with all objective functions, and the most expected range $1.5 < R_r\ [\Omega] < 4$ is selected;
- $\lambda_s + \lambda_r$ demonstrated a clear correlation with all objective functions, and its range was narrowed to exclude a local minimum as $32 < \lambda_s + \lambda_r\ [mH] < 51$;
- An inverse relationship was observed for R_m, where larger values consistently yielded smaller errors. The selected range is $500 < R_m\ [\Omega] < 20000$;
- L_m also showed a distinct correlation with almost all objective functions, clearly indicating the optimal search region of $0.25 < L_m\ [H] < 0.48$.

This sensitivity analysis transforms a broad, unconstrained optimization problem into a well-defined and constrained search, for an accurate final identification by the GA.

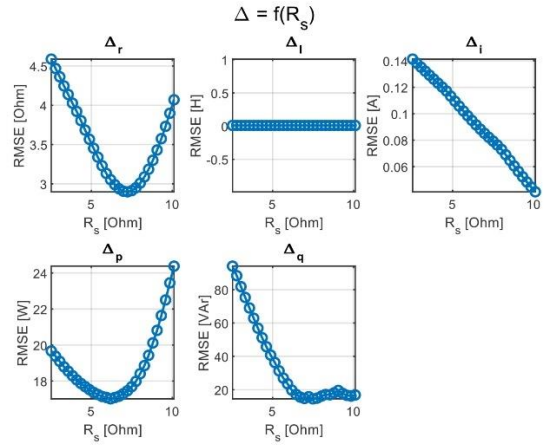

a)

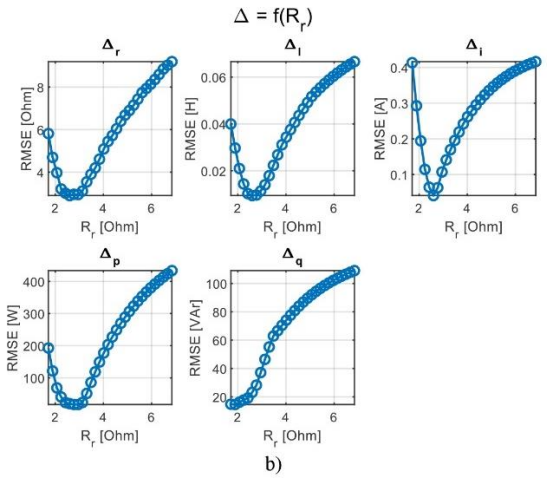

b)

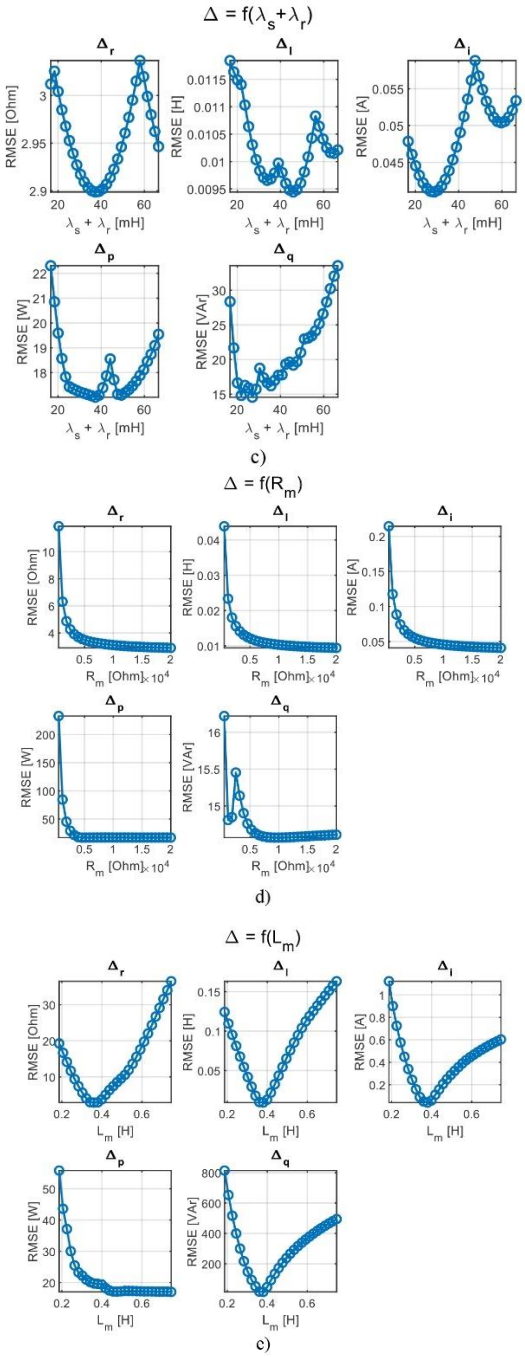

Fig. 6 Minimal obtainable specific RMSE for: a) R_s variation; b) R_r variation; c) $\lambda_s + \lambda_r$ variation; d) R_m variation; e) L_m variation

For the final, precise parameter identification, GA was employed using the boundaries identified in the previous stage. The five-error functions were combined into a single fitness function (15) for the GA. Specific weight factors used to create all expected errors in a similar order of magnitude for this specific case are selected as stated in (16):

$$w_r = 1, w_l = 100\pi, w_i = 1, w_p = 0.01, w_q = 0.01 \tag{16}$$

The use of these weighting factors is critical to normalize the individual error terms, which have different physical units and numerical scales, ensuring that no single objective function disproportionately influences the optimization process. These specific weighting factors apply to the induction motor of this specific size, and would differ for machines of different power.

The MATLAB Global Optimization Toolbox ga solver was used with a population size of 150 and a maximum of 1000 generations; the mutation operator was Adaptive Feasible, the function tolerance was set to $1 \cdot 10^{-5}$, and the run terminated early if no improvement was observed for 70 consecutive generations (stall generation limit). These settings were chosen to ensure a thorough exploration of the constrained search space while maintaining a reasonable computational time. The 'Adaptive Feasible' mutation function is particularly well-suited for this problem, as it respects the parameter boundaries established during the sensitivity analysis. The execution of this algorithm yields the final, optimized set of T-equivalent circuit parameters.

3. Results and Discussion

Validation used two complementary approaches to assess both static accuracy and dynamic fidelity. First, we benchmarked the identified parameters against those from conventional offline tests (IEEE 112), grounding the in-situ method in an industry standard and measuring direct agreement. Second—and most relevant for DT creation—we compared the DT's time-series outputs to measured data under real operating conditions. This evaluates the DT's ability to reproduce machine behavior over time; success here demonstrates practical utility for real-time monitoring, simulation, and predictive analysis.

3.1. Comparison with Standard Test Parameters

The parameters identified by the proposed GA-based method were compared against those obtained for the same IM using the conventional no-load and locked-rotor tests, prescribed by the IEEE Standard 112. The comparison provides a direct measure of the proposed method's ability to replicate the results of the industry-standard, offline procedure with a reduced testing procedure. The results of this comparison are presented in Table 2. In Table 2 are also added results from the GA algorithm that are not constrained by GS boundaries. From the aspect of computational expense, GS uses a considerable amount of resources in terms of memory and processing power and is related to grid density (number of points). In the paper, grid search space is divided among 30 points for each of 5 parameters, that results in $5 \cdot 30^5$ computational points. In MATLAB, double precision number requires 8 bytes, or about 970 MB of memory needed for storage of all results. When GS-defined boundaries are inserted into GA, it requires less time to reach the minimum obtainable error. GS computational complexity does not depend on the machine

size, only on grid density. Also, GS can be conducted only to establish a baseline, and afterwards, during routine check, or online parameter adaptation, only the GA part can be utilized. In Table 2 provided execution times are observed on PC with the following specification: Windows 11, CPU-AMD 7900X, RAM-32 GB DDR5, GPU-RTX 3060.

Table 2 reveals notable differences between the parameters identified by the proposed method and the standard offline tests. The R_s and $\lambda_s + \lambda_r$ values exhibit a significant deviation of approximately 50%, while R_r shows a more moderate discrepancy of around 25%. In contrast, L_m demonstrates strong agreement, with a difference of only 5%. These deviations may be attributed to the different operating conditions under which the parameters were identified; the proposed method uses real load points, while the standard tests operate at the extremes of no-load and locked-rotor, where effects like magnetic saturation can differ. The GA was run 20 consecutive times, and Table 2 shows mean values with Standard Deviation (SD) obtained from those tests.

The largest error is observed in the core loss resistance, R_m. It is important to note, however, that this parameter is frequently omitted altogether in many equivalent circuit models found in the literature due to its high variability and lesser impact on overall electromagnetic torque characteristics [31], [32]. Nevertheless, it should be noted that this approach does not provide an accurate estimation for the core loss resistance.

Table 2 IEEE 112 and GA results comparison

Method	IEEE 112	GS + GA (proposed method)		Plain GA	
Parameter	Value	Value (Mean ± SD)	Difference	Value (Mean ± SD)	Difference
Execution time (s)	/	90 s (GS) + 0.22 s (GA)		0.39 s	
R_s	5.053 [Ω]	7.36 ± 0.04 [Ω]	46%	8.24± 0.11 [Ω]	63%
R_r	3.422 [Ω]	2.66 ± 0.02 [Ω]	-22%	2.64± 0.02 [Ω]	-22%
$\lambda_s + \lambda_r$	33.2 [mH]	50.4 ± 1.02 [mH]	52%	51.1 ± 1.27 [mH]	54%
R_m	700 [Ω]	19.35 ± 0.04 [kΩ]	2664%	235 ± 112 [kΩ]	33471%
L_m	384 [mH]	369 ± 0.73 [mH]	-4%	367 ± 0.75 [mH]	-4%

3.2. Time-Series Performance Validation

To evaluate the practical effectiveness of the proposed technique, two distinct DT models were created in MATLAB. The first utilized the parameters identified via the in-situ GS+GA method, as presented in Table 2. The second was built using parameters obtained from the conventional IEEE 112 standard tests, serving as a benchmark. Both models were then fed the same recorded time-series data of measured phase voltages and rotor speed to compare their behavioral fidelity against the real-world measurements.

Fig. 7 and Fig. 8 provide a direct visual comparison of the time-series performance for phase current along with the calculated absolute error. Fig 9 and Fig. 10. provide a direct visual comparison of the time-series performance of active power and reactive power, along with calculated absolute error. As is evident from the figures, the DT created with the GA-identified parameters demonstrates a strong correspondence with the measured data across the majority of operating points in both motor and generator regimes. The DT based on the IEEE 112 parameters, while representing the machine's fundamental design characteristics, shows some variance from the operational data, particularly in the estimation of

active power and during certain transient phases. This highlights an important distinction in the purpose of the two parameter sets.

It is important to emphasize that the IEEE 112 standard provides a robust, repeatable, and essential method for determining a motor's fundamental parameters, which is critical for design, manufacturing, and acceptance testing. These tests, however, are performed under specific, controlled conditions (no-load and locked-rotor) that may not fully capture the nuanced behavior of a machine integrated into a system with a wide range of operational load points. In contrast, the proposed in-situ method is inherently tailored to the machine's "as-is" condition within its specific operational context. Therefore, it is a logical outcome that its resulting model provides a closer behavioral match to the operational data from which its parameters were derived. This suggests that for applications requiring a high-fidelity behavioral DT for real-time monitoring and "what-if" analysis, the in-situ identification approach is well-suited.

Notably, it must be acknowledged that both models exhibit increased deviation in the generator regime. This consistent discrepancy under specific conditions raises a pertinent question about the universal adequacy of the standard T-equivalent circuit itself for high-fidelity modeling across all possible operating quadrants, irrespective of the parameter identification method used.

3.3. Discussion on Parameter Accuracy vs. Behavioral Fidelity

The validation results present an interesting finding for the field of DT. On one hand, the parameter comparison in Table 2 shows significant deviations between the GA-identified parameters and those from the IEEE 112 tests. On the other hand, the time-series validation in Figs. 7 through 10 demonstrates that the DT built with these GA parameters has higher behavioral fidelity. This apparent contradiction highlights a key concept: the objective of the parameter identification method dictates the utility of its results. The IEEE 112 standard is designed to characterize a machine's fundamental properties under two specific, controlled, and extreme operating conditions (no-load and locked-rotor). While essential for design and acceptance testing, these parameters do not necessarily guarantee the most accurate behavioral model across a wide range of real-world load points.

In contrast, the proposed in-situ GA method is explicitly optimized to minimize the behavioral error across a set of actual, loaded operating points. The GA is effectively finding a "best fit" set of parameters that work together holistically to reproduce the IM's observed behavior, likely compensating for minor real-world effects not captured by the ideal T-equivalent circuit. Therefore, for the specific application of creating a DT for monitoring or simulation, the parameters are those that best reproduce the machine's behavior.

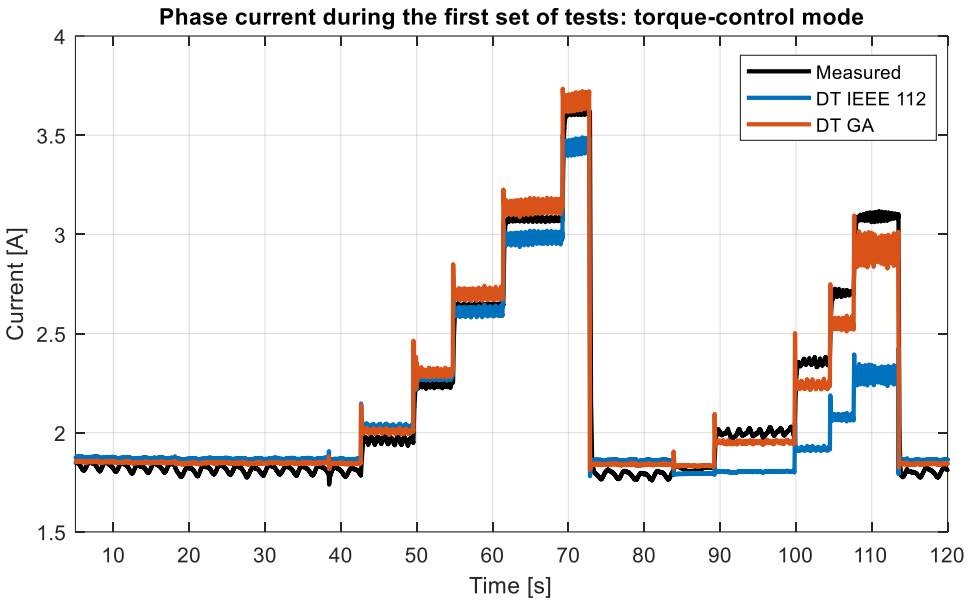

a)

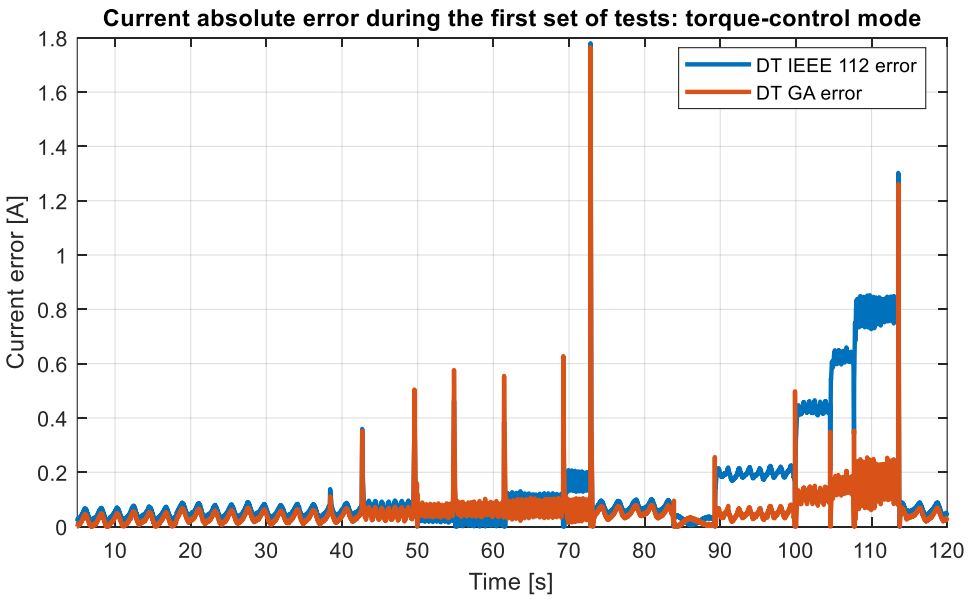

b)

Fig. 7 Comparison of measured and DT provided phase current of IM, first set of tests: a) measured and estimated data; b) absolute error

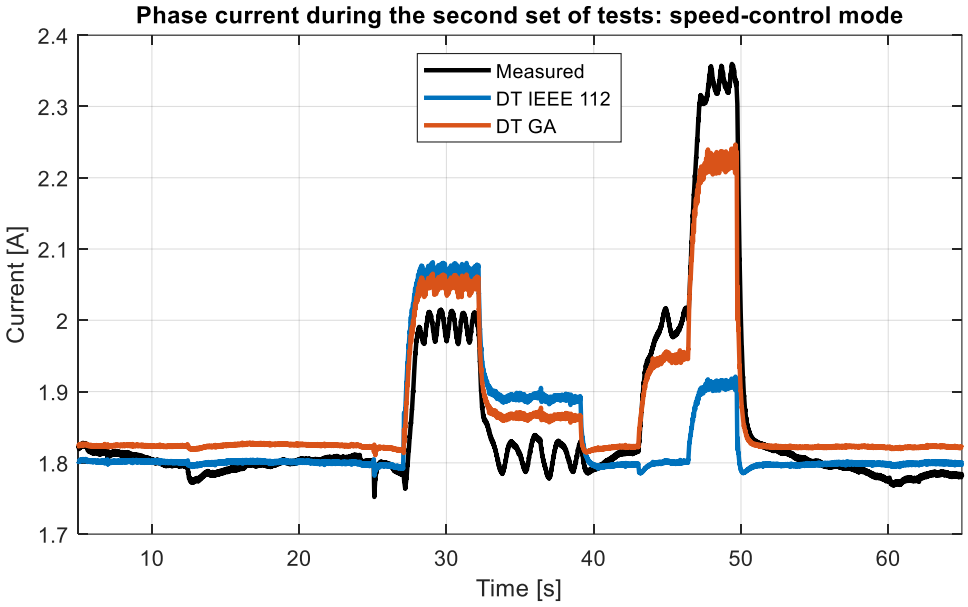

a)

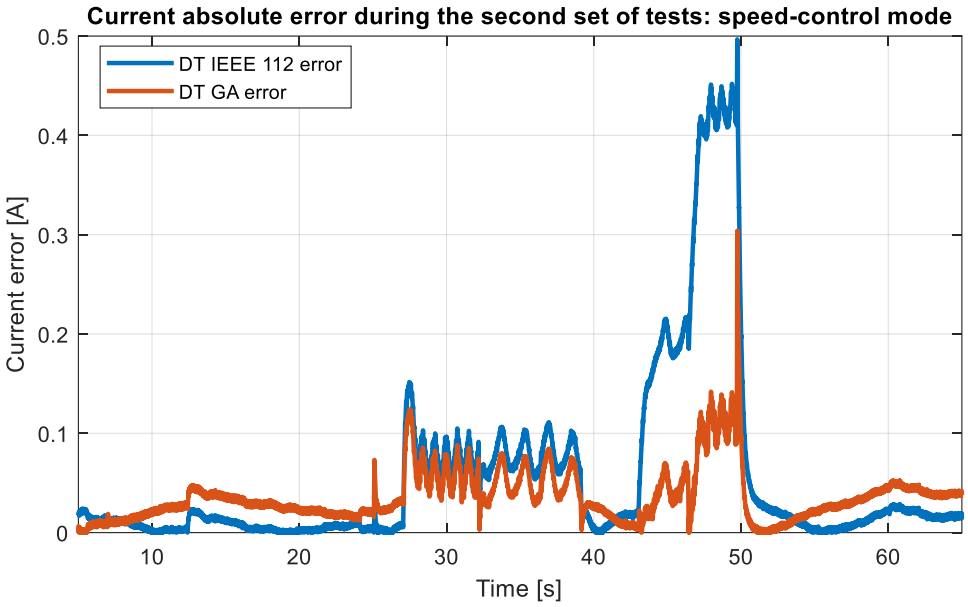

b)

Fig. 8 Comparison of measured and DT provided phase current of IM, second set of tests: a) measured and estimated data; b) absolute error

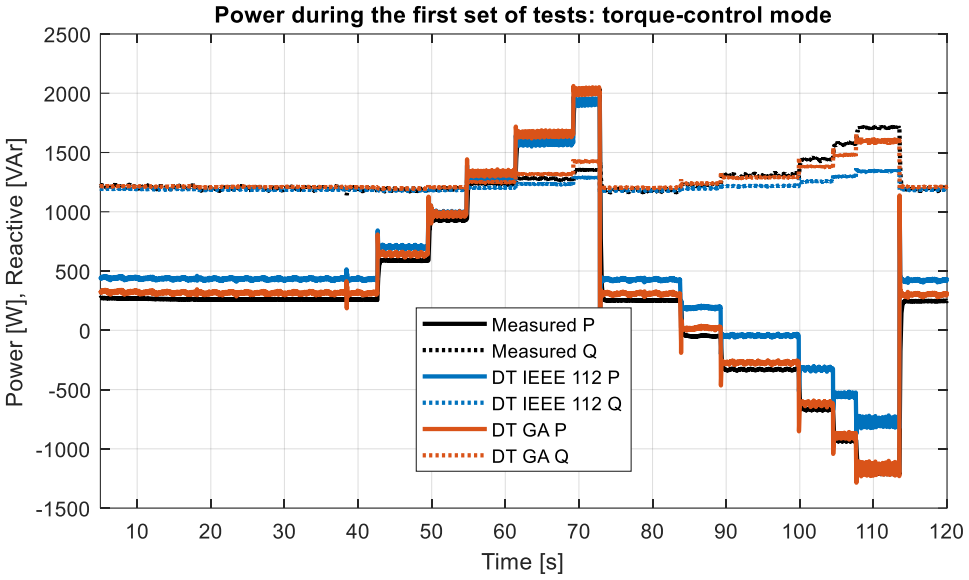

a)

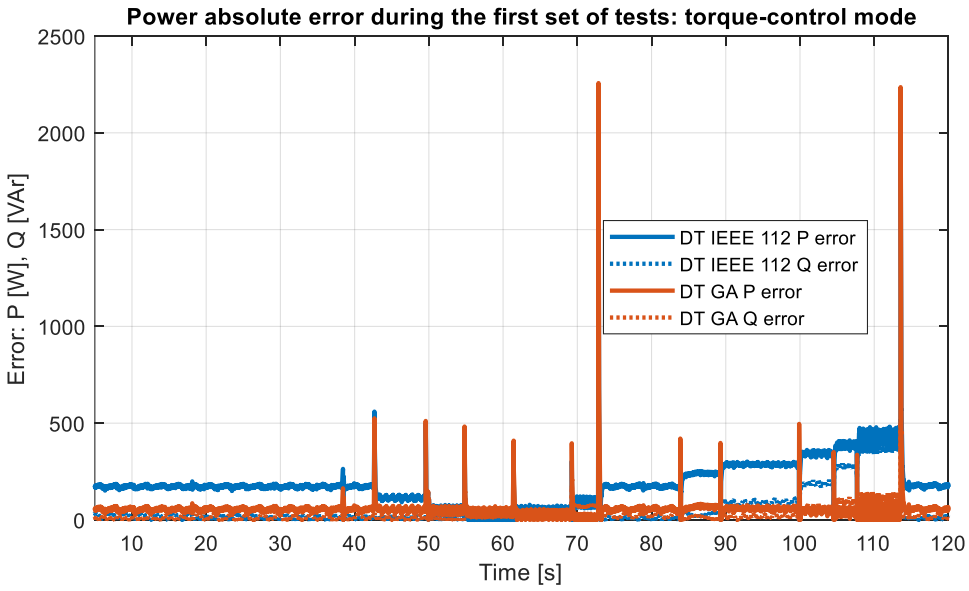

b)

Fig. 9 Comparison of measured and DT provided P and Q of IM, first set of tests: a) measured and estimated data; b) absolute error

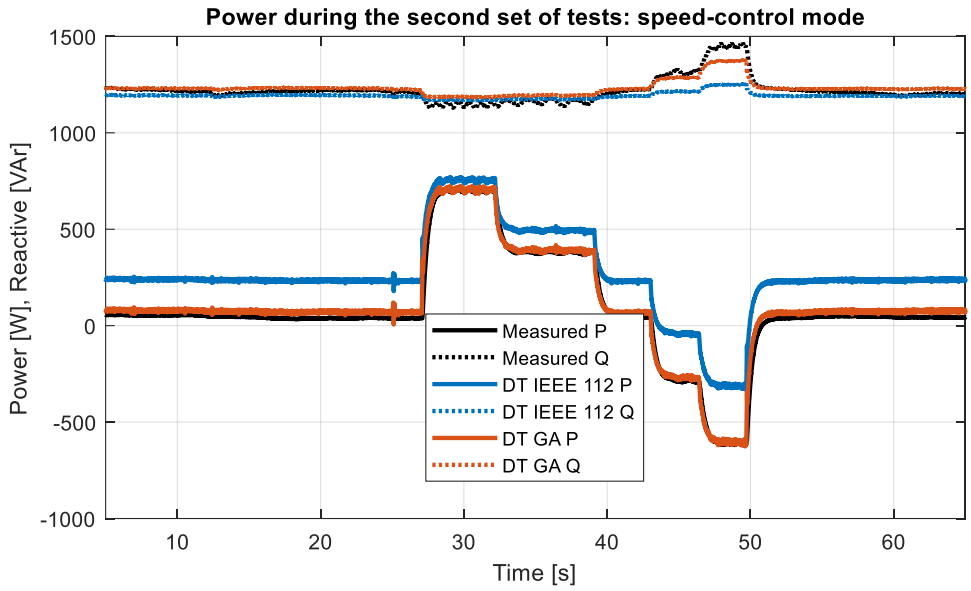

a)

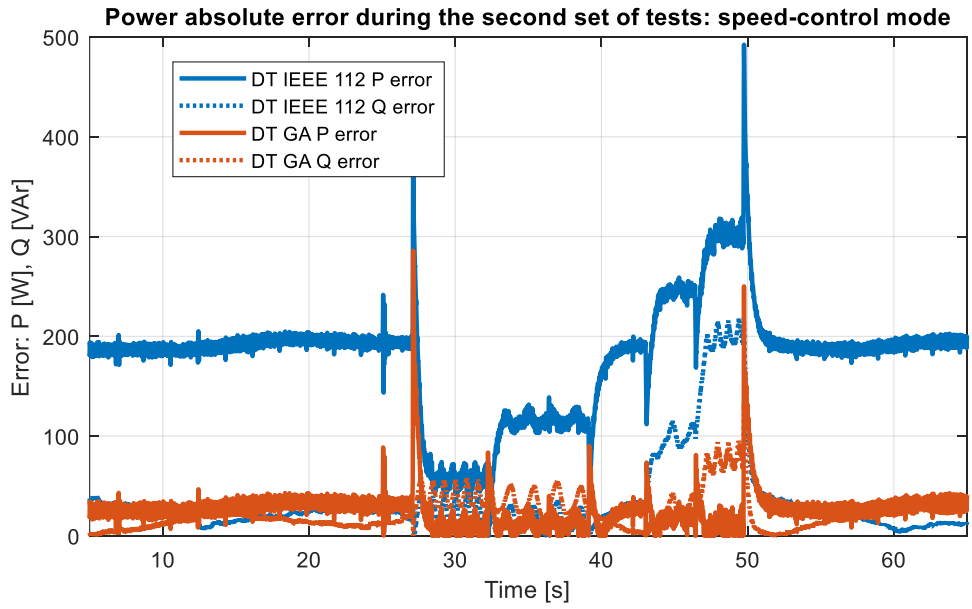

b)

Fig. 10 Comparison of measured and DT provided P and Q of IM, second set of tests: a) measured and estimated data; b) absolute error

3.4. Limitations of the proposed method

The proposed identification is steady-state and non-invasive; consequently, the following limitations apply:

1. Requirement of quasi steady-state – parameters are inferred from stationary plateaus; transient behaviour is not identified.
2. Limited observability of parameters – only the sum of leakage inductances is strongly observable; core loss resistance cannot be reliably identified and estimation carry large uncertainty.
3. Requirement of encoder – required for slip calculation and recorded data inherets encoder quantization and latency.
4. Requirement of balanced grid voltage condition – unbalance or harmonic distorted grid voltages break used equivalent circuit assumptions; overcoming of this problem would require sequence extraction and per sequence modeling.
5. Multiple operating points for better estimation are required – operation of IM on a single load point close to synchronous speed would worsen identifiability of parameters and increase uncertainty of prediction for unseen operating points.
6. Need for explicit model choise – specific IM model has to be selected to calculate the error metric based on it; machines with double cage or deep bars would require different model and it is up to the user to select the appropriate model.

4. CONCLUSION

This paper presents a novel, four-step workflow with two-stage methodology that enables a reduced testing procedure for induction machine parameter identification to create high-fidelity digital twin. The proposed method successfully overcomes the significant practical limitations of traditional offline tests by exclusively using easily accessible, steady-state operational data.

The core of the contribution is a hybrid optimisation approach that leverages a grid-based sensitivity analysis to establish robust and narrow search boundaries for a genetic algorithm. This ensures both accuracy and the reliability of all parameter estimation except core loss. The validation results demonstrate the effectiveness of the method. While some identified parameters show deviations from standard test results, the overall model faithfully reproduces the machine's behaviour, which is the primary goal for a high-fidelity digital twin. The resulting digital twin accurately replicated the real machine’s behaviour, as confirmed by the comparison plots of phase current and active and reactive power.

The primary significance of this work lies in providing a practical and non-invasive procedure that allows for the creation and updating of an induction machine digital twin without requiring a costly testing procedure.

Future work will focus on expanding this methodology to different induction machines and accommodate induction machines that operate on a few steady-state operating points. Also, transient states and mechanical subsystem could be included in the analysis to provide valuable information for more accurate parameter identification.

Acknowledgement: *This work has been supported by the Ministry of Science, Technological Development and Innovation of the Republic of Serbia [Grant Number:451-03-136/2025-03/200102]*

REFERENCES

[1] Y. Lu, C. Liu, K. I.-K. Wang, H. Huang, and X. Xu, "Digital Twin-driven smart manufacturing: Connotation, reference model, applications and research issues, " *Robot Comput Integr Manuf*, vol. 61, p. 101837, Feb. 2020.

[2] X. Zhang and W. Zhu, "Application framework of digital twin-driven product smart manufacturing system: A case study of aeroengine blade manufacturing, " *Int J Adv Robot Syst*, vol. 16, no. 5, Sep. 2019.

[3] Z. Liu, Z.-Q. Lang, Y. Gui, Y.-P. Zhu, and H. Laalej, "Digital twin-based anomaly detection for real-time tool condition monitoring in machining, " *J Manuf Syst*, vol. 75, pp. 163–173, Aug. 2024.

[4] H. Liu, M. Xia, D. Williams, J. Sun, and H. Yan, "Digital Twin-Driven Machine Condition Monitoring: A Literature Review," *J Sens*, vol. 2022, pp. 1–13, Jul. 2022.

[5] M. Averbukh and E. Lockshin, "Estimation of the Equivalent Circuit Parameters of Induction Motors by Laboratory Test," *Machines*, vol. 9, no. 12, p. 340, Dec. 2021.

[6] "IEEE Standard Test Procedure for Polyphase Induction Motors and Generators," Dec. 06, 2017, *IEEE, Piscataway, NJ, USA*.

[7] L. Peretti and M. Zigliotto, "Automatic procedure for induction motor parameter estimation at standstill," *IET Electr Power Appl*, vol. 6, no. 4, pp. 214–224, Apr. 2012.

[8] N. Mitrović, F. Filipović, B. Banković, V. Kostić, S. Štatkić, and J. Vukašinović, "Comparison of Self Commissioning Procedure for Frequency Controlled Induction Motor Drive Parameter Identification," in *Proceedings SAUM 2024*, University of Niš, Faculty of Electronic Engineering, Faculty of Mechanical Engineering, Niš, 2024, pp. 189–192

[9] S. A. Al-Jufout, W. H. Al-rousan, and C. Wang, "Optimization of Induction Motor Equivalent Circuit Parameter Estimation Based on Manufacturer's Data," *Energies (Basel)*, vol. 11, no. 7, p. 1792, Jul. 2018.

[10] J. S. Hsu, J. D. Kueck, M. Olszewski, D. A. Casada, P. J. Otaduy, and L. M. Tolbert, "Comparison of induction motor field efficiency evaluation methods," *IEEE Trans Ind Appl*, vol. 34, no. 1, pp. 117–125, 1998.

[11] D. A. De Souza *et al.*, "Identification by Recursive Least Squares With Kalman Filter (RLS-KF) Applied to a Robotic Manipulator," *IEEE Access*, vol. 9, pp. 63779–63789, 2021.

[12] U. Sengamalai, G. Anbazhagan, T. M. Thamizh Thentral, P. Vishnuram, T. Khurshaid, and S. Kamel, "Three Phase Induction Motor Drive: A Systematic Review on Dynamic Modeling, Parameter Estimation, and Control Schemes," *Energies (Basel)*, vol. 15, no. 21, p. 8260, Nov. 2022.

[13] H. R. Mohammadi and A. Akhavan, "Parameter Estimation of Three-Phase Induction Motor Using Hybrid of Genetic Algorithm and Particle Swarm Optimization," *Journal of Engineering*, vol. 2014, pp. 1–6, 2014.

[14] M. Göztaş, M. Çunkaş, and M. A. Şahman, "In-Situ Efficiency Estimation of Induction Motors Using Whale Optimization Algorithm," *Turkish Journal of Electrical Power and Energy Systems*, vol. 5, no. 2, pp. 114–124, Jun. 2025.

[15] M. N. Diarra, Y. Yao, Z. Li, M. Niasse, Y. Li, and H. Zhao, "In-Situ Efficiency Estimation of Induction Motors Based on Quantum Particle Swarm Optimization-Trust Region Algorithm (QPSO-TRA)," *Energies (Basel)*, vol. 15, no. 13, p. 4905, Jul. 2022.

[16] M. Ćalasan, M. Micev, Z. M. Ali, A. F. Zobaa, and S. H. E. Abdel Aleem, "Parameter Estimation of Induction Machine Single-Cage and Double-Cage Models Using a Hybrid Simulated Annealing–Evaporation Rate Water Cycle Algorithm," *Mathematics*, vol. 8, no. 6, p. 1024, Jun. 2020.

[17] S.-H. Lee, A. Yoo, H.-J. Lee, Y.-D. Yoon, and B.-M. Han, "Identification of Induction Motor Parameters at Standstill Based on Integral Calculation," *IEEE Trans Ind Appl*, vol. 53, no. 3, pp. 2130–2139, May 2017.

[18] I. Knežević, M. Ćalasan, and T. Dlabač, "Novel Analytical Approaches for Induction Machine Direct Start-up Speed–Time Curve Modeling under Fan Load," *Electrical Engineering*, vol. 106, no. 2, pp. 1925–1938, Apr. 2024.

[19] L. V. Trieu, T. M. Pham, A. Hoang, and S. T. Nguyen, "Improved Parameter Estimation of Three-Phase Squirrel-Cage Induction Motors Using the Nelder-Mead Simplex Algorithm," *International journal of electrical and computer engineering systems*, vol. 15, no. 8, pp. 695–703, Sep. 2024.

[20] A. Charette, J. Xu, A. Ba-Razzouk, P. Pillay, and V. Rajagopalan, "The use of the genetic algorithm for in-situ efficiency measurement of an induction motor," in Proceedings of the 2000 IEEE Power Engineering Society Winter Meeting. Conference Proceedings (Cat. No.00CH37077), IEEE, pp. 392–397.

[21] J. Rengifo, E. Albanez, J. Benzaquen, A. Bueno, and J. M. Aller, "Full-Load Range In-Situ Efficiency Estimation Method for Induction Motors Using Only A Direct Start-Up," in Proceedings of the 2018 XIII International Conference on Electrical Machines (ICEM), IEEE, Sep. 2018, pp. 1213–1219.

[22] A. Amadou Adamou and C. Alaoui, "Energy efficiency model-based Digital shadow for Induction motors: Towards the implementation of a Digital Twin," *Engineering Science and Technology, an International Journal*, vol. 44, p. 101469, Aug. 2023.

[23] A. A. Adamou, C. Alaoui, M. Moustapha Diop, and A. Skorek, "Squirrel Cage Induction Motors Accurate Modelling for Digital Twin Applications," *Modelling*, vol. 5, no. 4, pp. 1582–1600, Oct. 2024.
[24] T. D. Lopes, A. Raizer, and W. Valente Júnior, "The Use of Digital Twins in Finite Element for the Study of Induction Motors Faults," *Sensors*, vol. 21, no. 23, p. 7833, Nov. 2021.
[25] "A Digital Twin Design of Induction Motor With Squirrel-Cage Rotor for Insulation Condition Prediction," *International Journal of Mechatronics and Applied Mechanics*, vol. I, no. 14, Nov. 2023.
[26] F. Filipović, M. Petronijević, N. Mitrović, B. Banković, and V. Kostić, "Benchmarking of Phase Lock Loop based Synchronization Algorithms for Grid-Tied Inverter," *Serbian Journal of Electrical Engineering*, vol. 16, no. 1, pp. 1–19, 2019.
[27] Z. Ali, N. Christofides, L. Hadjidemetriou, E. Kyriakides, Y. Yang, and F. Blaabjerg, "Three-phase phase-locked loop synchronization algorithms for grid-connected renewable energy systems: A review," *Renewable and Sustainable Energy Reviews*, vol. 90, pp. 434–452, Jul. 2018.
[28] A. Hace, "The Improved Division-Less MT-Type Velocity Estimation Algorithm for Low-Cost FPGAs," *Electronics (Basel)*, vol. 8, no. 3, p. 361, Mar. 2019.
[29] S. W. Smith, *The scientist and engineer's guide to digital signal processing*. 1997.
[30] S. A. Al-Jufout, W. H. Al-rousan, and C. Wang, "Optimization of Induction Motor Equivalent Circuit Parameter Estimation Based on Manufacturer's Data," *Energies (Basel)*, vol. 11, no. 7, p. 1792, Jul.
[31] P. Krause, O. Wasynczuk, S. Sudhoff, and S. Pekarek, Eds., *Analysis of Electric Machinery and Drive Systems*. Wiley, 2013. doi: 10.1002/9781118524336.
[32] J. Holtz, "Sensorless control of induction motor drives, " In Proceedings of the IEEE, vol. 90, no. 8, pp. 1359–1394, Aug. 2002.